Phase Diagram of Pyrochlore Iridates: All-in–All-out Magnetic Ordering and Non-Fermi-Liquid Properties

Hiroshi Shinaoka,[1,2] Shintaro Hoshino,[3,2] Matthias Troyer,[1] and Philipp Werner[2]
[1]*Theoretische Physik, ETH Zürich, 8093 Zürich, Switzerland*
[2]*Department of Physics, University of Fribourg, 1700 Fribourg, Switzerland*
[3]*Department of Basic Science, The University of Tokyo, Meguro 153-8902, Japan*
(Received 21 April 2015; revised manuscript received 10 August 2015; published 7 October 2015)

We study the prototype $5d$ pyrochlore iridate $Y_2Ir_2O_7$ from first principles using the local density approximation and dynamical mean-field theory (LDA + DMFT). We map out the phase diagram in the space of temperature, on-site Coulomb repulsion U, and filling. Consistent with experiments, we find that an all-in–all-out ordered insulating phase is stable for realistic values of U. The trigonal crystal field enhances the hybridization between the $j_{\mathrm{eff}} = 1/2$ and $j_{\mathrm{eff}} = 3/2$ states, and strong interband correlations are induced by the Coulomb interaction, which indicates that a three-band description is important. We demonstrate a substantial band narrowing in the paramagnetic metallic phase and non-Fermi-liquid behavior in the electron- or hole-doped system originating from long-lived quasi-spin-moments induced by nearly flat bands.

DOI: 10.1103/PhysRevLett.115.156401 PACS numbers: 71.15.Mb, 71.15.Rf, 71.27.+a, 71.30.+h

The competition and cooperation between spin-orbit coupling (SOC) and electron correlations induces novel phenomena in $4d$ and $5d$ transition metal oxides such as spin-orbit-assisted Mott insulators, topological phases, and spin liquids [1]. The pyrochlore iridates $A_2Ir_2O_7$ (A = Pr, Nd, Y, etc.) are an ideal system to study these phenomena because their magnetic and electronic states can be tuned by chemical substitution, pressure, and temperature (T). Furthermore, intriguing phenomena such as correlated topological phases have been theoretically predicted on their geometrically frustrated crystal structure [1].

In 2001, it was reported that these compounds show a crossover from metal to insulator with decreasing A^{3+} ionic radii at high T [2] and a magnetic anomaly was found at low T for small A^{3+} ionic radii [3]. For the metallic compound A = Pr, experiments revealed spin-liquid behavior [4,5] and an unconventional anomalous Hall effect [6]. On the other hand, the Ir magnetic ordering has not been determined for a decade due to the strong neutron absorption by Ir and large magnetic contributions from rare-earth f moments on A^{3+}. The magnetic order has only recently been identified as a noncollinear all-in–all-out order [see Fig. 1(a)] [7–9].

Among the insulating compounds, $Y_2Ir_2O_7$ has the highest magnetic transition temperature and no f moments. This makes this compound a prototype system for studying strong electron correlations among $5d$ electrons. A pioneering local density approximation (LDA) + U study for this compound showed that the all-in–all-out order is indeed stable at large on-site repulsion U [10]. It also proposed a topological Weyl semimetal as the ground state of some compounds in this series. This stimulated further theoretical studies on the topological nature and unconventional quantum criticality of $5d$ electrons on the pyrochlore lattice [1,11–19].

In pyrochlore iridates, the Ir atoms form a frustrated pyrochlore lattice, a corner-sharing network of tetrahedra [see Fig. 1(a) and Ref. [20]]. The so-called $j_{\mathrm{eff}} = 1/2$ picture was originally proposed for the insulating quasi-2D compound Sr_2IrO_4 with the same electron configuration $5d^5$ [21,22]. The SOC splits the t_{2g} manifold into a fully occupied $j_{\mathrm{eff}} = 3/2$ quartet and a half-filled $j_{\mathrm{eff}} = 1/2$ doublet ($\hat{j}_{\mathrm{eff}} \equiv \hat{S} - \hat{L}$ is the effective total angular momentum, $\hat{S}$ and $\hat{L}$ the spin and orbital momenta). This picture was subsequently confirmed by LDA + dynamical

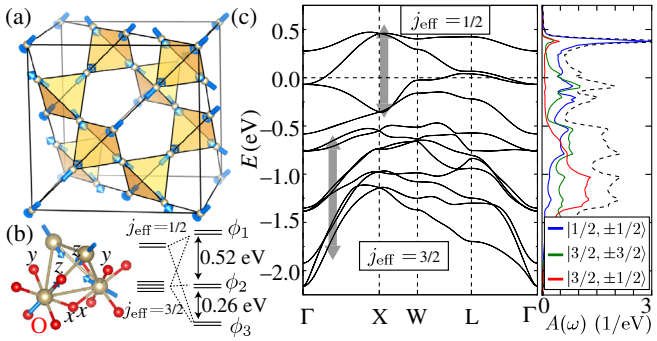

FIG. 1 (color online). (a) Pyrochlore lattice formed by Ir atoms with arrows representing spin moments in the all-in–all-out magnetic structure. (b) fcc unit cell with the local coordinate axes and the energy diagram under SOC (ζ) and the trigonal crystal field (Δ_{tri}). (c) LDA band structure together with the density of states projected on the j_{eff} basis. The broken line shows the total density of states. The $j_{\mathrm{eff}} = 1/2$ and $j_{\mathrm{eff}} = 3/2$ bands consist mainly of the $j_{\mathrm{eff}} = 1/2$ and $j_{\mathrm{eff}} = 3/2$ manifolds, but they are substantially hybridized under the trigonal CF (see the text).

mean-field theory (DMFT) studies [23–25]. The $j_{\rm eff} = 1/2$ and $3/2$ manifolds hybridize either under a tetragonal crystal field (CF), as in the case of Sr_2IrO_4, or under a trigonal CF because they do not commute with $\hat{j}^2_{\rm eff}$. For pyrochlore iridates, a recent quantum chemistry calculation found that the trigonal CF is comparable to the SOC [26]. Moreover, the t_{2g} band width in the LDA band structure ($\simeq$2 eV [27]) is even smaller than the typical value of U for Ir^{4+} ($\simeq$3 eV [28]). These effects will enhance the hybridization between the two $j_{\rm eff}$ manifolds beyond the single-particle level, raising questions about the validity of the $j_{\rm eff} = 1/2$ single-band picture. Another interesting issue is the role of the geometrical frustration, which suppresses long-range magnetic ordering and induces a novel type of magnetism [20]. To address these questions, it is important to perform a first-principles study of the three-band system which takes into account SOC, electron correlations, itinerancy, and the crystal structure.

In this Letter, we present state-of-the-art relativistic LDA + DMFT calculations for the prototypical compound $Y_2Ir_2O_7$. We map out the phase diagram in T and on-site Coulomb repulsion U and investigate the properties of the correlated $5d$ electrons in this family. First, we construct maximally localized Wannier functions for the t_{2g} manifold [29] using an LDA exchange-correlation functional [30,31]. We use the code QMAS (quantum materials simulator) [32], which is based on the projector augmented wave method [33], and the two-component formalism [34,35]. The experimental crystal structure at 290 K is taken from Ref. [36]. In our DMFT calculations, electron correlation effects are taken into account by introducing the Slater-Kanamori interaction

$$H_{\rm int} = \frac{1}{2} \sum_{\alpha\beta\alpha'\beta'\sigma\sigma'} U_{\alpha\beta\alpha'\beta'} c^\dagger_{i\alpha\sigma} c^\dagger_{i\beta\sigma'} c_{i\beta'\sigma'} c_{i\alpha'\sigma} \qquad (1)$$

in the standard parametrization $U_{\alpha\alpha\alpha\alpha} = U$, $U_{\alpha\beta\alpha\beta} = U - 2J_H$, $U_{\alpha\beta\beta\alpha} = U_{\alpha\alpha\beta\beta} = J_H$ ($\alpha \neq \beta$), with α (β) and σ (σ') being orbital and spin indices, respectively. U and J_H are the on-site repulsion and the Hund's coupling, respectively. We choose $J_H/U = 0.1$, which is motivated by a first-principles estimate for the related compound Na_2IrO_3 ($U = 2.72$ eV, $J_H = 0.23$ eV) [28]. Within DMFT, one has to solve a three-orbital quantum impurity problem with off-diagonal and complex hybridization functions. We employ a numerically exact continuous-time quantum Monte Carlo impurity solver based on the hybridization expansion [37,38]. In previous studies, the quantum impurity models for $5d$ electrons have been simplified to avoid a severe sign problem, e.g., by omitting off-diagonal hybridization functions and some interaction terms in the $j_{\rm eff}$ basis [39]. Since pyrochlore iridates have large interband hybridizations, we solve our impurity problem without such approximations. Another advantage of this treatment is that we do not need to assume the quantization axes of spin and orbital. The sign problem is reduced by rotating the single-particle basis of the hybridization function [40]. Please refer to the Supplemental Material [41] for technical details and some results on the effects of the off-diagonal hybridizations.

Figure 1(c) shows the computed LDA band structure. The upper half-filled manifold, which is usually identified as the $j_{\rm eff} = 1/2$ manifold, has an overlap with the lower manifold in energy space, although the bands are separated at each k point. The $j_{\rm eff} = 1/2$ manifold has four Kramers degenerate bands since a unit cell contains four Ir atoms. We constructed a tight-binding model based on t_{2g}-orbital-like maximally localized Wannier functions. The SOC ζ and the trigonal crystal field $\Delta_{\rm tri}$ are estimated to be $\zeta = 0.40$ eV and $\Delta_{\rm tri} = 0.23$ eV [42]. These values are consistent with an estimate by a quantum chemistry calculation [26]. As shown in Fig. 1(b), the t_{2g} manifold splits into three doublets under ζ and $\Delta_{\rm tri}$. The wave function of the highest doublet ϕ_1 is given by $\phi_{1\pm} = -0.977|1/2, \pm 1/2\rangle - 0.212|3/2, \pm 1/2\rangle$ in the $j_{\rm eff}$ basis $|j_{\rm eff}, j^{111}_{\rm eff}\rangle$. We denote by $\hat{j}^{111}_{\rm eff}$ the effective angular momentum along the local [111] axis [see Fig. 1(a)]. The $|1/2, \pm 1/2\rangle$ states have spin and orbital moments reduced by 29% from the ideal atomic values $1/3\mu_B$ and $2/3\mu_B$, because the Wannier functions have substantial weight on neighboring oxygen atoms. On the other hand, the magnetic moments are enhanced by the hybridization between the $j_{\rm eff} = 1/2$ and $j_{\rm eff} = 3/2$ manifolds by $\Delta_{\rm tri}$. As a result, the doublet ϕ_1 has spin and orbital moments of $0.490\mu_B$ and $0.598\mu_B$. To illustrate the effects of itinerancy, we plot the density of states projected on the $j_{\rm eff}$ basis. The contributions of $|1/2, \pm 1/2\rangle$ and $|3/2, \pm 3/2\rangle$, which are not mixed by $\Delta_{\rm tri}$, have comparable weight near the Fermi level, which indicates that the interatomic hybridization also plays a substantial role.

Next, we discuss the U-T phase diagram obtained by the DMFT calculations [Fig. 2(a)]. There is a dome-shaped all-in–all-out magnetically ordered phase at large U. The transition temperature T_c rises up to values about three times higher than the experimental $T_c^{\rm exp} \lesssim 150$ K. This may be due to the neglect of spatial fluctuations in the DMFT approximation. We show the T-dependent spin and orbital moments along the local [111] axis (m_{111} and L_{111}) computed at several values of U in Fig. 2(b). Both order parameters emerge concurrently with the same sign. The Ir magnetic moment is estimated to be $0.93\mu_B$ at low T for $U = 2.5$ eV, which is larger than an experimental estimate of the upper bound ($0.5\mu_B$) [36]. The ratio $L_{111}/m_{111} \simeq 1.2$ is substantially smaller than $L_{111}/m_{111} = 2$ of the $j_{\rm eff} = 1/2$ state. By contrast, a LDA + DMFT study estimated $L_{111}/m_{111} \simeq 2.2$ for Sr_2IrO_4 [25]. On the other hand, the spectral weight $A(\omega = 0)$ shows a drop at T_c for $U = 2$ eV, signaling a transition from a paramagnetic metal into an all-in–all-out ordered insulator. At higher U ($\geq$2.5 eV), the spectral function is substantially suppressed even above T_c, indicating that the system is in a Mott insulating state. A crossover between a paramagnetic metal and a paramagnetic insulator is located around

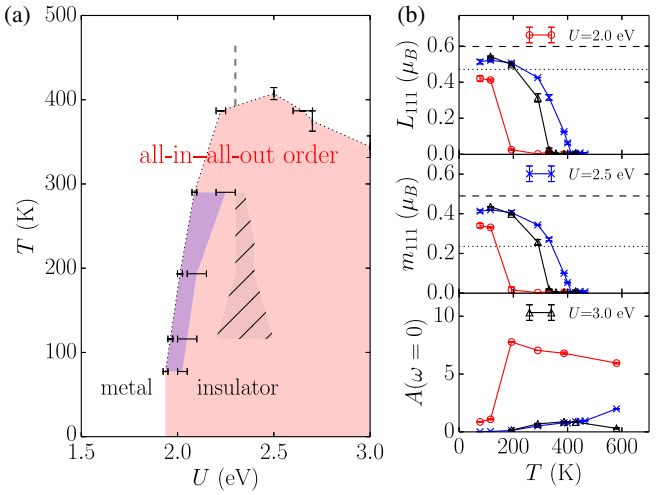

FIG. 2 (color online). (a) U-T phase diagram at half filling. There is a first-order transition between the magnetic insulator and the paramagnetic metal at low T and small U. The blue shaded region denotes the hysteresis region associated with this transition. The error bars reflect the uncertainty caused by the finite number of parameter values considered. The metal-insulator crossover in the high-T paramagnetic phase is shown by a broken line. The hashed region represents the first-order Mott transition and its hysteresis region in paramagnetic DMFT calculations. (b) temperature dependence of the angular and magnetic moments along the local [111] axis and the spectral weight at $\omega = 0$ for half filling. The moment values of the $j_{\mathrm{eff}} = 1/2$ and ϕ_1 doublets are shown by dotted and broken lines, respectively (see the text).

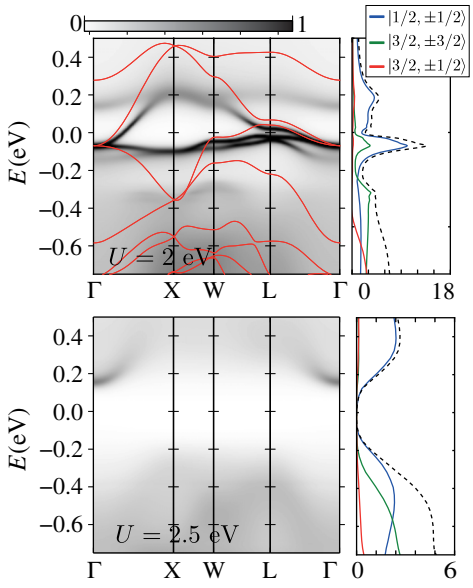

FIG. 3 (color online). Momentum-resolved spectral function $A(k,\omega)$ at $U = 2$ eV (paramagnetic metal) and $U = 2.5$ eV (all-in–all-out ordered insulator) at 290 K. The LDA band structure is shown by red lines. On the right we plot the k-integrated spectral function projected on the j_{eff} basis (the broken line is the total spectral function).

$U = 2.3$ eV at high T. In Fig. 2(a), we also show the first-order Mott transition line obtained by paramagnetic DMFT calculations. Apparently, the metal-insulator transition in the magnetic DMFT phase diagram is assisted by magnetic ordering. The insulating compound $Y_2Ir_2O_7$, which has the highest T_c in the family, may be located at $U \simeq 2.5$ eV.

At low T and small U, we find a first-order transition between the paramagnetic metallic phase and the all-in–all-out ordered insulating phase (both states are topologically trivial). For $Nd_2Ir_2O_7$, it was reported that its magnetic and metal-insulator transition at $T_c = 33$ K is second order [43]. The first-order nature may be an artifact of the LDA + DMFT method. A previous LDA + U study found a Weyl semimetallic phase on the lower-U side of an all-in–all-out ordered insulating phase [10]. In our DMFT phase diagram, however, the semimetallic phase is taken over by the insulating phase and there is a direct transition between the paramagnetic metal and the magnetic insulator. This appears to be a strong correlation effect.

Figure 3 shows the spectral function $A(k,\omega)$ computed for $T = 290$ K. At $U = 2$ eV (paramagnetic metal), the upper manifold near the Fermi level shows a substantial band narrowing from the LDA value of $\simeq 1$ eV down to approximately 0.4 eV, while the lower manifold is smeared out by correlation effects. The low-energy states consist mainly of the $j_{\mathrm{eff}} = 1/2$ orbitals for $\omega > 0$. A similar purification of the spectral function was found in LDA + DMFT studies of Sr_2IrO_4. At $U = 2$ eV and $U = 2.5$ eV (all-in–all-out ordered insulator), no clear separation is seen between the $j_{\mathrm{eff}} = 1/2$ and $j_{\mathrm{eff}} = 3/2$ manifolds in the total spectral function $A(\omega)$.

We now investigate the effect of doping this insulating solution. The electron filling n is changed from 4.6 to 5.8 ($n = 5$ corresponds to the undoped compound). The all-in–all-out order vanishes rapidly upon electron or hole doping at $n = 4.8$ and $n = 5.2$, respectively. We plot $\mathrm{Im}\Sigma(i\omega_n)$ in Fig. 4(a) for $n = 4.6$ and $n = 5.6$. In a Fermi liquid, $\mathrm{Im}\Sigma(i\omega_n)$ vanishes linearly with ω_n at low frequencies (i.e., $\propto \omega_n^{\alpha}$ with $\alpha = 1$) when T is sufficiently low. However, for a rather wide range of frequencies, our data show that $\mathrm{Im}\Sigma(i\omega_n)$ vanishes more slowly in the doped insulator. We estimated the exponent α using the lowest two Matsubara frequencies assuming $\mathrm{Im}\Sigma(i\omega_n) = \beta\omega_n^{\alpha}$. The result is shown in Fig. 4(b) for different values of n. One sees a substantial reduction of α from 1 around $n = 4.6$ and $n = 5.8$. This non-Fermi-liquid (NFL) or bad metallic behavior persists down to the lowest temperature considered (77 K).

Theoretically, it has been reported that NFL behavior with a reduced power-law exponent in the frequency-dependent self-energy can be induced by the Hund coupling in multiorbital systems [44–46]. In the latter case, $\mathrm{Im}\Sigma(i\omega_n)$ shows a nonzero intersect as $\omega_n \to 0$ close to half filling, and a fractional power-law scaling appears at the boundary between the NFL regime and the Fermi-liquid regime [44]. This sharp crossover has been coined the "spin-freezing transition," because the scattering in the NFL state is related to the appearance of long-lived local moments. To see if the NFL behavior in the pyrochlore

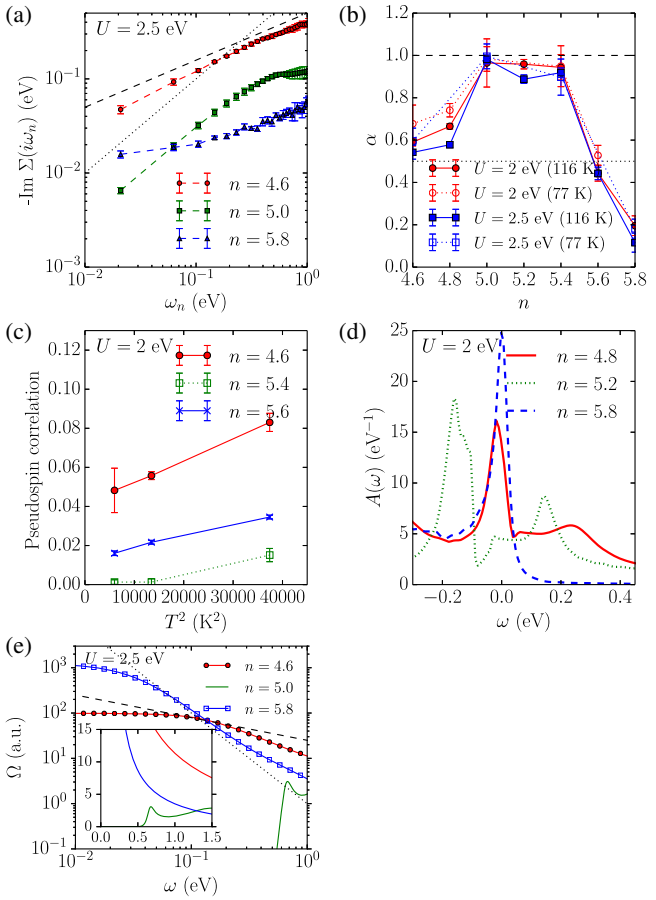

FIG. 4 (color online). (a) Frequency dependence of the imaginary part of the self-energy projected on the $j_{\rm eff} = 1/2$ manifold. The dotted and broken lines are $\propto \omega_n$ and $\propto \omega_n^{0.5}$, respectively. n is the number of electrons in the t_{2g} shell ($n = 5$ is the undoped case). (b) n dependence of the exponent α [$\mathrm{Im}\Sigma(i\omega_n) \propto \omega_n^{\alpha}$]. (c) T dependence of the imaginary-time pseudospin correlation at $\tau = \beta/2$ (see the text for the definition). (d) Spectral functions computed at 116 K. (e) Optical conductivity $\Omega(\omega)$. The dotted and broken lines are $\propto \omega^{-2}$ and $\propto \omega^{-0.5}$, respectively.

iridates has a similar origin, we plot in Fig. 4(c) the imaginary-time correlator $\langle \hat{s}^{\rm quasi}(\tau = \beta/2)\hat{s}^{\rm quasi}(\tau = 0)\rangle$ computed for $U = 2$ eV, where the quasi spin is defined for the highest ϕ_1 doublet as $\hat{s}^{\rm quasi} = \hat{n}_{\phi_{1+}} - \hat{n}_{\phi_{1-}}$. As can be seen, this correlation function extrapolates to a finite value as $T \to 0$ for $n = 4.6$ and $n = 5.8$, indicating the existence of long-lived quasi-spin-moments. However, these long-lived moments are not a consequence of the Hund coupling; they rather originate from properties of the band dispersion, i.e., crystal structure, which we confirmed by reproducing this NFL behavior even with J_H turned off (not shown).

As illustrated in Fig. 4(d), $A(\omega)$ shows two characteristic peaks at the upper and lower edges of the $j_{\rm eff} = 1/2$ manifold at $n = 5.2$ (electron-doped Fermi liquid). These two peaks come from nearly flat quasiparticle bands in the paramagnetic phase [Fig. 3(a)], corresponding to peak structures seen in the LDA density of states [Fig. 1]. The NFL behavior appears when the Fermi level hits one of these peaks. This leads to the formation of local moments and a reduction of the coherence temperature T^*.

One might wonder if the NFL state is stable against magnetic ordering other than the all-in–all-out order. We confirmed that the NFL state is stable by performing DMFT calculations without assuming the all-in–all-out magnetic ordering down to 116 K. This robustness is likely due to the geometrically frustrated crystal structure which prevents long-range ordering. The NFL state may be observed by optical conductivity measurements [e.g., $\alpha = 0.5$ implies an optical conductivity $\Omega(\omega) \propto 1/\sqrt{\omega}$ [44]], or by the T dependence of the resistivity. Figure 4(e) shows the optical conductivity $\Omega(\omega)$ along [001] computed at $U = 2.5$ eV and 116 K. The ω dependence deviates substantially from the Fermi-liquid-like behavior ω^{-2} for the hole-doped case $n = 4.6$ around $\omega = 1$ eV. On the other hand, the conductivity of the electron-doped compound $n = 5.8$ is closer to an ω^{-2} behavior, which is likely due to the small self-energy [see Fig. 4(a)]. It was reported that the undoped metallic $Bi_2Ir_2O_7$ shows a bad metallic behavior and the transport properties sensitively depend on the magnetic field [47]. That paper discussed the connection between these nontrivial properties and a sharp peak in the LDA density of states near the Fermi level. Although this compound has a wider band width and is considered to be weakly correlated, it would be interesting to investigate it with LDA + DMFT.

In summary, we have mapped out the finite-T phase diagram of the $5d$ pyrochlore iridate $Y_2Ir_2O_7$ using a state-of-the-art relativistic LDA + DMFT approach. We showed that the spin and orbital moments are substantially enhanced by the trigonal crystal field and that the $j_{\rm eff} = 1/2$ picture is not valid. We have also identified a characteristic non-Fermi-liquid self-energy which originates from long-lived quasi-spin-moments induced by nearly flat bands. Because of experimental difficulties such as the lack of a natural cleavage plane, angle-resolved photoemission data of this family have been reported only for $Bi_2Ir_2O_7$ [48]. However, the connection of the non-Fermi-liquid behavior to nearly flat bands enables an analysis of the electronic structure by macroscopic measurements. Although the hole-doped compounds $Ca_xY_{2-x}Ir_2O_7$ show a bad metallic behavior for $x > 0.3$ [49,50], the nature of this metallic state remains to be clarified. It would be interesting to explore the optical conductivity or T-dependent resistivity of these doped compounds to confirm the NFL behavior. A comparative study with the osmate $Cd_2Os_2O_7$ with a $5d^3$ configuration would also be interesting [51–54].

We thank Lewin Boehnke, Xi Dai, Li Huang, Hugo Strand, Jakub Imriska, Yukitoshi Motome, Hongbin Zhang, Youhei Yamaji, Lei Wang, and Hiroshi Watanabe for the stimulating discussions and useful comments. We thank Jakxub Imriska for the use of his code for matrix manipulations. We also thank Kentarou Ueda and Jun Fujioka for the discussions on their experimental data and Shoji Ishibashi for providing the pseudopotentials.

We acknowledge support from the DFG via FOR 1346, the SNF Grant No. 200021E-149122, ERC Advanced Grant SIMCOFE and NCCR MARVEL. The calculations have been performed on the Mönch and Brutus clusters of ETH Zürich using codes based on ALPS [55]. The crystal structure was visualized using VESTA3 [56].

[1] W. Witczak-Krempa, G. Chen, Y. B. Kim, and L. Balents, Annu. Rev. Condens. Matter Phys. **5**, 57 (2014).
[2] D. Yanagishima and Y. Maeno, J. Phys. Soc. Jpn. **70**, 2880 (2001).
[3] N. Taira, M. Wakeshima, and Y. Hinatsu, J. Phys. Condens. Matter **13**, 5527 (2001).
[4] S. Nakatsuji, Y. Machida, Y. Maeno, T. Tayama, T. Sakakibara, J. van Duijn, L. Balicas, J. N. Millican, R. T. Macaluso, and J. Y. Chan, Phys. Rev. Lett. **96**, 087204 (2006).
[5] Y. Tokiwa, J. J. Ishikawa, S. Nakatsuji, and P. Gegenwart, Nat. Mater. **13**, 356 (2014).
[6] Y. Machida, S. Nakatsuji, Y. Maeno, T. Tayama, T. Sakakibara, and S. Onoda, Phys. Rev. Lett. **98**, 057203 (2007).
[7] K. Tomiyasu, K. Matsuhira, K. Iwasa, M. Watahiki, S. Takagi, M. Wakeshima, Y. Hinatsu, M. Yokoyama, K. Ohoyama, and K. Yamada, J. Phys. Soc. Jpn. **81**, 034709 (2012).
[8] H. Sagayama, D. Uematsu, T. Arima, K. Sugimoto, J. J. Ishikawa, E. O'Farrell, and S. Nakatsuji, Phys. Rev. B **87**, 100403 (2013).
[9] S. M. Disseler, Phys. Rev. B **89**, 140413 (2014).
[10] X. Wan, A. M. Turner, A. Vishwanath, and S. Y. Savrasov, Phys. Rev. B **83**, 205101 (2011).
[11] B.-J. Yang and Y. B. Kim, Phys. Rev. B **82**, 085111 (2010).
[12] M. Kargarian, J. Wen, and G. A. Fiete, Phys. Rev. B **83**, 165112 (2011).
[13] G. Chen and M. Hermele, Phys. Rev. B **86**, 235129 (2012).
[14] W. Witczak-Krempa, A. Go, and Y. B. Kim, Phys. Rev. B **87**, 155101 (2013).
[15] E.-G. Moon, C. Xu, Y. B. Kim, and L. Balents, Phys. Rev. Lett. **111**, 206401 (2013).
[16] A. Go, W. Witczak-Krempa, G. S. Jeon, K. Park, and Y. B. Kim, Phys. Rev. Lett. **109**, 066401 (2012).
[17] S. B. Lee, A. Paramekanti, and Y. B. Kim, Phys. Rev. Lett. **111**, 196601 (2013).
[18] L. Savary, E.-G. Moon, and L. Balents, Phys. Rev. X **4**, 041027 (2014).
[19] T. Bzdušek, A. Rüegg, and M. Sigrist, Phys. Rev. B **91**, 165105 (2015).
[20] J. S. Gardner, M. J. P. Gingras, and J. E. Greedan, Rev. Mod. Phys. **82**, 53 (2010).
[21] B. J. Kim, H. Jin, S. J. Moon, J. Y. Kim, B. G. Park, C. S. Leem, J. Yu, T. W. Noh, C. Kim, S. J. Oh, J. H. Park, V. Durairaj, G. Cao, and E. Rotenberg, Phys. Rev. Lett. **101**, 076402 (2008).
[22] B. J. Kim, H. Ohsumi, T. Komesu, S. Sakai, T. Morita, H. Takagi, and T. Arima, Science **323**, 1329 (2009).
[23] C. Martins, M. Aichhorn, L. Vaugier, and S. Biermann, Phys. Rev. Lett. **107**, 266404 (2011).
[24] R. Arita, J. Kuneš, A. V. Kozhevnikov, A. G. Eguiluz, and M. Imada, Phys. Rev. Lett. **108**, 086403 (2012).
[25] H. Zhang, K. Haule, and D. Vanderbilt, Phys. Rev. Lett. **111**, 246402 (2013).
[26] L. Hozoi, H. Gretarsson, J. P. Clancy, B. G. Jeon, B. Lee, K. H. Kim, V. Yushankhai, P. Fulde, D. Casa, T. Gog, J. Kim, A. H. Said, M. H. Upton, Y.-J. Kim, and J. van den Brink, Phys. Rev. B **89**, 115111 (2014).
[27] R. S. Singh, V. R. R. Medicherla, K. Maiti, and E. V. Sampathkumaran, Phys. Rev. B **77**, 201102 (2008).
[28] Y. Yamaji, Y. Nomura, M. Kurita, R. Arita, and M. Imada, Phys. Rev. Lett. **113**, 107201 (2014).
[29] For technical details, see H. Shinaoka, Y. Motome, T. Miyake, and S. Ishibashi, Phys. Rev. B **88**, 174422 (2013).
[30] D. M. Ceperley and B. J. Alder, Phys. Rev. Lett. **45**, 566 (1980).
[31] J. P. Perdew and A. Zunger, Phys. Rev. B **23**, 5048 (1981).
[32] See http://qmas.jp/.
[33] P. E. Blöchl, Phys. Rev. B **50**, 17953 (1994).
[34] T. Kosugi, T. Miyake, and S. Ishibashi, J. Phys. Soc. Jpn. **80**, 074713 (2011).
[35] T. Oda, A. Pasquarello, and R. Car, Phys. Rev. Lett. **80**, 3622 (1998).
[36] M. C. Shapiro, S. C. Riggs, M. B. Stone, C. R. de la Cruz, S. Chi, A. A. Podlesnyak, and I. R. Fisher, Phys. Rev. B **85**, 214434 (2012).
[37] P. Werner, A. Comanac, L. de' Medici, M. Troyer, and A. Millis, Phys. Rev. Lett. **97**, 076405 (2006).
[38] P. Werner and A. J. Millis, Phys. Rev. B **74**, 155107 (2006).
[39] X. Dai (private communication).
[40] Refer to Appendix B in H. Shinaoka, M. Troyer, and P. Werner, Phys. Rev. B **91**, 245156 (2015).
[41] See Supplemental Material at http://link.aps.org/supplemental/10.1103/PhysRevLett.115.156401 for technical details and effects of off-diagonal hybridization functions.
[42] We used the same notation in Ref. [29].
[43] K. Matsuhira, M. Wakeshima, Y. Hinatsu, and S. Takagi, J. Phys. Soc. Jpn. **80**, 094701 (2011).
[44] P. Werner, E. Gull, M. Troyer, and A. J. Millis, Phys. Rev. Lett. **101**, 166405 (2008).
[45] L. de' Medici, J. Mravlje, and A. Georges, Phys. Rev. Lett. **107**, 256401 (2011).
[46] A. Georges, L. de' Medici, and J. Mravlje, Annu. Rev. Condens. Matter Phys. **4**, 137 (2013).
[47] T. F. Qi, O. B. Korneta, X. Wan, L. E. DeLong, P. Schlottmann, and G. Cao, J. Phys. Condens. Matter **24**, 345601 (2012).
[48] Q. Wang, Y. Cao, X. G. Wan, and J. D. Denlinger, J. Phys. Condens. Matter **27**, 015502 (2015).
[49] H. Fukazawa and Y. Maeno, J. Phys. Soc. Jpn. **71**, 2578 (2002).
[50] W. K. Zhu, M. Wang, B. Seradjeh, F. Yang, and S. X. Zhang, Phys. Rev. B **90**, 054419 (2014).
[51] H. Shinaoka, T. Miyake, and S. Ishibashi, Phys. Rev. Lett. **108**, 247204 (2012).
[52] J. Yamaura, K. Ohgushi, H. Ohsumi, T. Hasegawa, I. Yamauchi, K. Sugimoto, S. Takeshita, A. Tokuda, M. Takata, M. Udagawa, M. Takigawa, H. Harima, T. Arima, and Z. Hiroi, Phys. Rev. Lett. **108**, 247205 (2012).
[53] Z. Hiroi, J. Yamaura, T. Hirose, I. Nagashima, and Y. Okamoto, APL Mater. **3**, 041501 (2015).
[54] S. Tardif, S. Takeshita, H. Ohsumi, J.-i. Yamaura, D. Okuyama, Z. Hiroi, M. Takata, and T.-h. Arima, Phys. Rev. Lett. **114**, 147205 (2015).
[55] B. Bauer, L. D. Carr, H. G. Evertz, A. Feiguin, J. Freire, S. Fuchs, L. Gamper, J. Gukelberger, E. Gull, and S. Guertler, J. Stat. Mech. (2011) P05001.
[56] K. Momma and F. Izumi, J. Appl. Crystallogr. **44**, 1272 (2011).